

Determination of real-time predictors of the wind turbine wake meandering

Yann-Aël Muller · Sandrine Aubrun · Christian Masson

Received: 24 July 2014 / Revised: 3 January 2015 / Accepted: 16 February 2015 / Published online: 3 March 2015
© Springer-Verlag Berlin Heidelberg 2015

Abstract The present work proposes an experimental methodology to characterize the unsteady properties of a wind turbine wake, called *meandering*, and particularly its ability to follow the large-scale motions induced by large turbulent eddies contained in the approach flow. The measurements were made in an atmospheric boundary layer wind tunnel. The wind turbine model is based on the actuator disc concept. One part of the work has been dedicated to the development of a methodology for horizontal wake tracking by mean of a transverse hot wire rake, whose dynamic response is adequate for spectral analysis. Spectral coherence analysis shows that the horizontal position of the wake correlates well with the upstream transverse velocity, especially for wavelength larger than three times the diameter of the disc but less so for smaller scales. Therefore, it is concluded that the wake is actually a rather passive tracer of the large surrounding turbulent structures. The influence of the rotor size and downstream distance on the wake meandering is studied. The fluctuations of the lateral force and the yawing torque affecting the wind turbine model are also measured and correlated with the wake meandering. Two approach flow configurations are then tested: an undisturbed incoming flow (modelled atmospheric boundary layer) and a disturbed incoming flow, with a wind turbine model located upstream. Results showed that the meandering process is amplified by the presence of the upstream wake. It is shown that the coherence between

the lateral force fluctuations and the horizontal wake position is significant up to length scales larger than twice the wind turbine model diameter. This leads to the conclusion that the lateral force is a better candidate than the upstream transverse velocity to predict in real time the meandering process, for either undisturbed (wake free) or disturbed incoming atmospheric flows.

List of symbols

a	Axial induction factor
Δy	Transverse spacing between the probes that constitute the hot wire rake
α	Power law exponent
C_T	Thrust coefficient
D	Disc diameter
Du_i	Local velocity deficit at the i th probe position
f	Frequency
H_{hub}	Disc “hub height”
I_u	Turbulent intensity for the axial velocity component defined as $I_u = \sigma_u/U$
I_w	Turbulent intensity for the vertical velocity component defined as $I_w = \sigma_w/U$
L	Streamwise distance between the disc and the hot wire rake
L_{ux}	Integral scale for the axial velocity component
L_{wx}	Integral scale for the vertical velocity component
u, v, w	Instantaneous wind velocity along x, y and z axis respectively
u^*	Friction velocity
U	Time-averaged velocity
U_∞	Upstream time-averaged velocity at hub height
v_{upstream}	Upstream transverse velocity fluctuation
$v_{\text{downstream}}$	Downstream transverse velocity fluctuation
y_{wake}	Transverse wake position fluctuation

Y.-A. Muller · S. Aubrun (✉)
Univ. Orléans, INSA-CVL, PRISME EA-4229, 8, rue Léonard de Vinci, 45072 Orléans Cedex 2, France
e-mail: sandrine.aubrun@univ-orleans.fr

C. Masson
Ecole de Technologie Supérieure, 1100, rue Notre-Dame Ouest, Montréal H3C 1K3, Canada

z_0 Roughness length

1 Introduction

Wind turbine wake interactions are one source of power losses in wind farms, and they are so far poorly predicted since the wake models implemented in commercial wind resource assessment models are very basic. On the other hand, some recent studies proposed some improved wake models compared to those of Ainslie (1988) and Jensen (1983) which give acceptable results even in cases of multiple wakes in wind farms (Frandsen et al. 2006). The unsteady behaviour of the wind turbine far wake is not yet implemented in these models, because they are mainly dedicated to the determination of the production loss due to wake interactions. If one focuses on the aero-elasticity issues and the additional fatigue due to wake interactions, the implementation of unsteady wake models is necessary (Larsen et al. 2008, 2013; Trujillo and Kühn 2009). Indeed, the unsteady behaviour of the wake called *meandering*, in which the whole wake is seen to oscillate randomly albeit with a prevalence to in the horizontal plane, has been observed (Taylor et al. 1985) and captured (Bingöl et al. 2010; Trujillo et al. 2011) during field experiments. In all the above cited works, It is presumed that the large-scale turbulent eddies contained in the atmospheric boundary layer are responsible of this meandering, whereas the smaller turbulent eddies contribute to the turbulent diffusion of the far wake. It should be mentioned that other sources of wake meandering may exist as for example periodic vortex shedding in cases where the rotor acts as a bluff body due to a very high axial induction factor, high solidity (Cannon et al. 1993), or a massive hub (Medici and Alfredsson 2006). Other causes for the meandering may include instabilities from the hub or tip vortices (Chamorro et al. 2013; Iungo et al. 2013; Felli et al. 2011). The meandering originating from these phenomena is generally characterized by a sharp-frequency signature. These potential sources of meandering do not exist with the actuator disc that is being used in this work, and thus are not presently studied. This work instead focuses on the study of the meandering as an effect of the large scales of the atmospheric turbulence, which do not present a characteristic frequency. In the case of a real full-scale turbine, several of those causes for the meandering may be present at once.

The *Dynamic Wake Meandering* model by Larsen et al. (2008) proposes to split the large and small turbulent scales at twice the wind turbine wake diameter. This assumption, completed by the Taylor hypothesis of frozen turbulence, gives the possibility of generating a transfer function between the incoming velocity fluctuations and the meandering process. As will be seen, this rough separation

between the turbulent scales responsible for the meandering and the others is not realistic and could be improved by characterizing the correlated scales through dedicated wind tunnel experiments. It is one goal of the present paper.

Another potential benefit of this strategy is to use this procedure in real time on production sites in order to improve the wind farm monitoring and control. Having a measurement of the upstream wind conditions could help predict at a very short timescale the incoming flow fluctuations and the subsequent wake meandering. They could furthermore be integrated into the wind turbine control systems. On the other hand, it is not yet common to have access to the measurements of the incoming flow of a wind turbine, even though the LiDAR technology is now mature enough to potentially enable the development of some LiDAR-assisted control systems (Cholbrock et al. 2013; Davoust et al. 2014). One of our goals is to determine a potentially better candidate than the incoming flow velocity as meandering predictor. It is expected that the global unsteady aerodynamic loads applied to the wind turbine, which equate to an integrated indicator of the inhomogeneous velocity fluctuations impacting the rotor, could be adapted to this issue (Hu et al. 2012), and an experiment has been designed in order to prove this expectation.

To obtain this information, experiments were performed in an atmospheric boundary layer wind tunnel at a reduced scale of 1:400, in which the turbulent properties of the modelled boundary layer are representative of the atmosphere in neutral stability conditions over a moderately rough terrain. The wind turbines are modelled through the actuator disc concept with a porous disc made of metallic mesh, ensuring a good representation of the wind turbine far wake. España et al. (2011, 2012) and Aubrun et al. (2013) already proved that the meandering process could be observed and quantified with this set-up. It ensures also the absence of rotational effects, tip vortices, and vortex shedding that could be encountered with a rotating wind turbine (Zhang et al. 2012, 2013; Hancock and Pascheke 2014). A modelled wind turbine is fixed on a 6-axis unsteady aerodynamic balance. A specific signal processing technique based on the synchronous measurements of five single component hot wire probes horizontally aligned downstream of the modelled wind turbine was designed in order to track in real time the wind turbine wake transverse position. The spectral content of the incoming flow fluctuations, the global load fluctuations, and the instantaneous wake position are discussed, and the coherence functions between one another is then studied in order to identify the best candidate to predict in real time the meandering behaviour of the wake. Two different upstream conditions are compared (non-disturbed atmospheric boundary layer flow or disturbed with an incoming wind turbine wake).

2 Experimental set-up

The experiments were carried out in the “Lucien Malavard” wind tunnel located at the PRISME Laboratory from the University of Orleans (Fig. 1). The wind tunnel is equipped for modelling a neutrally stratified ABL flow at a geometric scale of 1:400. In order to obtain a model of a moderately rough atmospheric boundary layer, the 14-m development

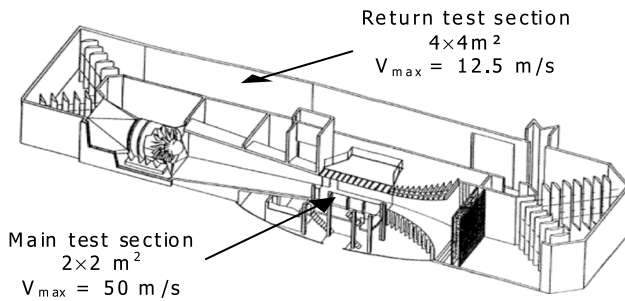
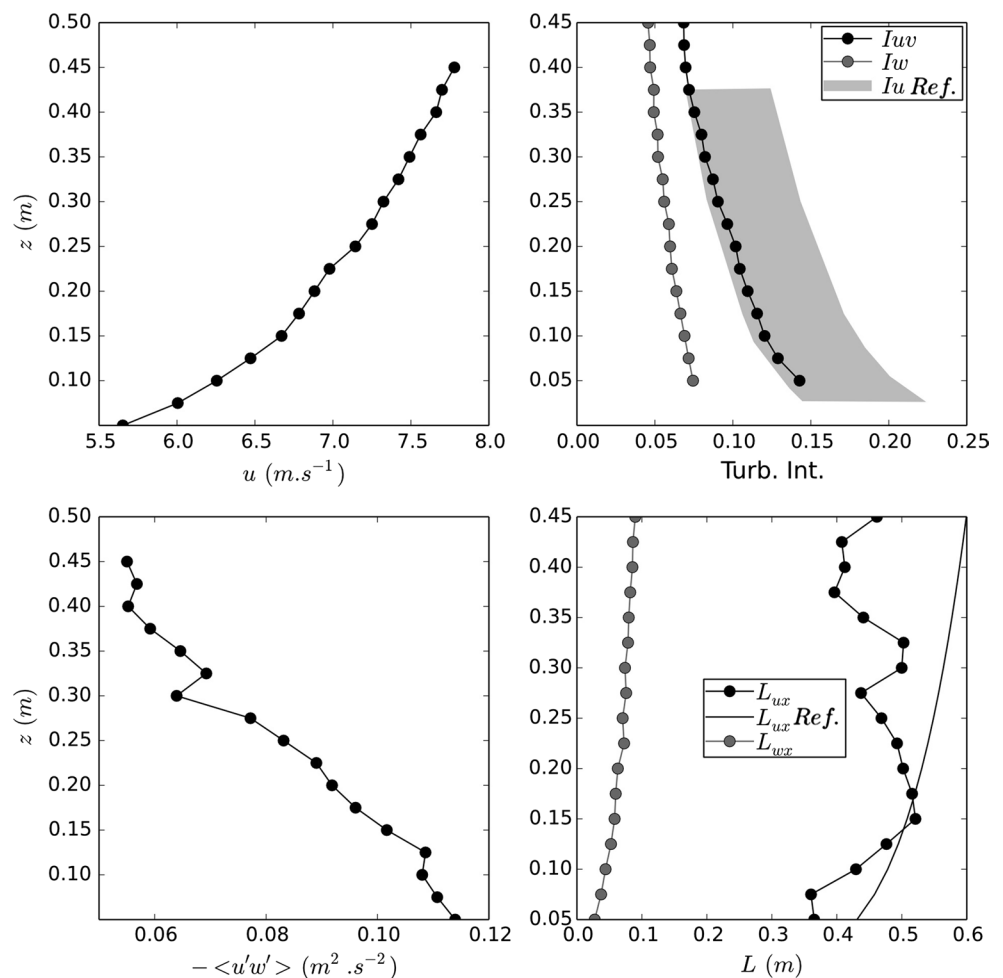


Fig. 1 The “Lucien Malavard” wind tunnel of PRISME Laboratory, University of Orléans. Measurements were performed in the return test circuit, adapted to model a neutrally stratified atmospheric boundary layer

plate is covered with perforated steel sheet. Furthermore a turbulence grid, combined with turbulence generators, is located at the entrance of the wind tunnel section in order to initiate appropriate mean velocity and turbulence intensity profiles. Although the return test section is 4 m × 4 m, the effective test area is 3 m wide and 1.5 m high.

Properties of the obtained boundary layer (mean velocity, turbulence intensity, and integral length scale profiles) are checked at the end of the 14-m fetch and are in agreement with the standards for atmospheric boundary layers flows (Counihan 1975; Snyder 1981; ESDU 1985; Kaimal and Finnigan 1994; VDI 2000) (Fig. 2). The ABL is representative of a moderately rough terrain, with a roughness length of $z_0 = 5.10^{-5}$ m (equivalent full-scale roughness length of 0.02 m), a power law exponent of $\alpha = 0.14$, and a friction velocity of $u^* = 0.29$ m s⁻¹. The turbulence intensity profiles are within the expected range for this type of terrain, and the expected ratio between the turbulence intensities $I_w/I_u = 0.5$ is obtained. The streamwise integral length scale $L_{u,x}$ is relatively constant at the height of interest and is 2–4 times larger than the rotor diameter (the integral timescales were determined as the time delay

Fig. 2 Vertical profiles of the approach flow conditions. *Upper left* the mean streamwise velocity; *upper right* the streamwise and vertical turbulence intensities, with the standard range proposed by the VDI for a moderately rough ABL; *lower left* the Reynolds stress; *lower right* the streamwise integral length scales, along with the scaled down reference profile obtained from Counihan for a roughness $z_0 = 0.02$



for which the autocorrelation functions of the velocity fluctuations is equal to $1/e$ and converted to length scales with the Taylor hypothesis). This ensures that the meandering process due to the presence of large turbulent eddies in the incoming flow can exist.

The modelling concept of the wind turbine is based on the actuator disc theory as described by Aubrun et al. (2007). The rotor is reproduced with a disc of metallic mesh of 100 or 200 mm of diameter (D) (40 or 80 m at full scale, respectively). The solidity of the porous disc is 45 % (wire diameter of 1 mm and thread spacing of 3.2 mm), leading to an equivalent axial induction factor of 0.19 and a thrust coefficient of $C_T = 0.62$. The value for the axial induction factor is obtained thanks to its definition: $a = 1/2(1 - U_w/U_\infty)$ where U_w is the minimum velocity measured within the wake of the porous disc (methodology described in Aubrun et al. 2007). The value for the thrust coefficient is obtained from the axial induction factor thanks to Froude's actuator disc theory, where $C_T = 4a(1 - a)$. The centre of the porous disc is located at a variable hub height H_{hub} with a threaded rod with a $0.05D$ diameter.

A horizontal hot wire rake composed of five hot wire probes (four 55P11 single probes, one 55P61 X-probe and anemometers from Dantec Dynamics) located at a distance L downstream of the wind turbine is used to determine the instantaneous horizontal wake position (Fig. 3).

The hot wires are calibrated using the Dantec hot wire calibration unit with the Streamware acquisition software. The calibration uses a fifth-order polynomial fitted on five calibration points spread logarithmically 0.5 and 10 m s⁻¹.

The choice is made to focus the whole study on the horizontal meandering only since it has been observed that it is the main meandering direction due to the horizontal turbulent velocity fluctuations in a turbulent boundary layer being larger than the vertical ones, which is itself

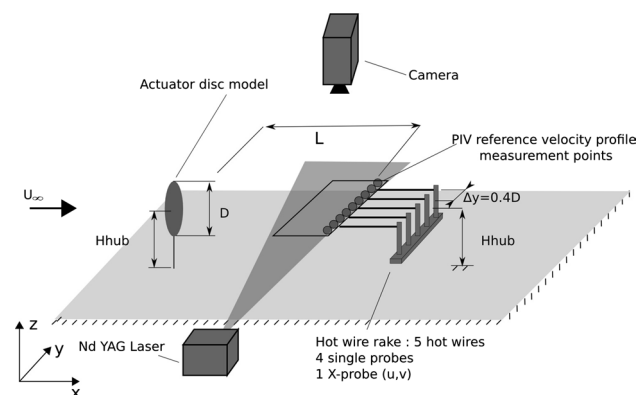


Fig. 3 Experimental set-up used for the validation of the wake tracking methodology

a consequence of the effect of blockage by the ground (Kaimal and Finnigan 1994; España et al. 2011).

On one side of the rake, the X hot wire probe is used in order to measure the local transverse velocity fluctuations. The uniform spacing between probes is Δy . Several values between $0.3D$ and $0.5D$ have been tested for Δy with no significant difference in the results. The methodology to calculate the horizontal wake position is based on the calculation of a weighted average of the location of each probe (which is fixed), where the weighting is chosen as the exponential of the instantaneous local velocity deficit, for the N profile points:

$$y_{\text{wake}}(t) = \left(\sum_{i=1}^N \exp(Du_i(t)) \times y_i \right) / \sum_{i=1}^N \exp(Du_i(t)) \quad (1)$$

The local velocity deficit, Du_i , for each data point is defined as the difference between the local velocity and the maximum velocity in the profile, as shown on Fig. 4 for the hot wire data.

In order to validate the methodology, a TSI 2D2C PIV system is also used to simultaneously measure the instantaneous velocity profiles at the level of the hot wire rake (see Fig. 3 for the set-up and Table 1 for the acquisition properties). The flow was seeded with a fine mist of olive oil (1 μm diameter). The area of interest was illuminated by use of an Nd-YAG twin laser, model CFR PIV 190 manufactured by Big Sky Laser (now Quantel) to generate a laser light sheet. The images were acquired with a POWERVIEW Plus 4 M camera with a resolution of 2048×2048 pixels. Signal acquisition and processing of raw data was performed using the software TSI Insight

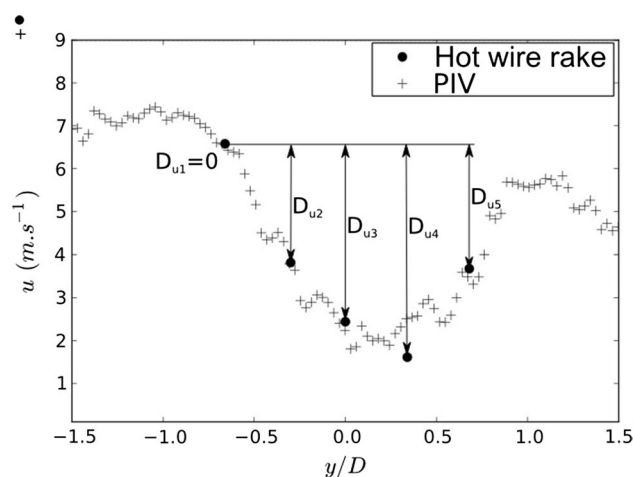


Fig. 4 Example of instantaneous velocity profiles from hot wire and PIV measurements, with the velocity deficits and reference velocity highlighted for the hot wire profile

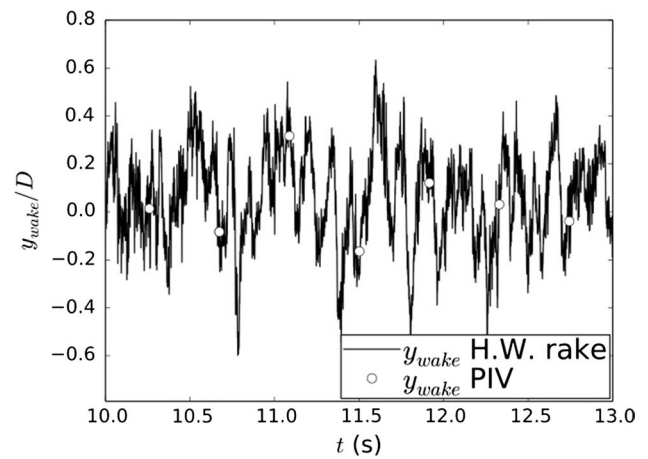
Table 1 Acquisition properties used on hot wire rake and PIV system during the validation of the wake tracking methodology

Acquisition systems characteristics	Hot wire rake	PIV
Resolution	5 Points	96 Points
F_{acq}	20 kHz	2.4 Hz
Samples	4,000,000	450

4G. The calibration was performed by using the TSI Dual Plane/Dual Sided calibration target. The image correlations are performed in two passes. The size of the interrogation windows is 64×64 pixels for the first pass and 32×32 for the second pass with an overlap of 25 %. The exact displacements were then determined by fitting the correlation fields with a Gaussian window. The synchronization pulses from the PIV synchronizer were also acquired along with the hot wire time series so as to allow time correlations between the different data sources.

For the validation (case 0), a disc diameter of $D = 100$ mm is used. Since the velocity profiles from the hot wire rake and from the PIV system are synchronous, it is possible to compare the results of the wake position detection method on the data sets originating from both sources according to Eq. (1). In the case of the PIV, the number of profile points is $N = 96$, whereas for the hot wire data, the number of profile points is $N = 5$. The choice of an exponential weighting function gives an increased weight to the maximum values of the velocity deficit, whereas linear weighting would yield the median value of the velocity deficit instead, splitting its area in half. This weighting function is chosen empirically, so as to provide the best agreement between the two wake position series in spite of the widely different number of data points. The wake position time series originating from spatially sparse hot wire data is then plotted along with the accurate wake position time series from spatially rich PIV data on Fig. 5. It appears that the wake positions from both data sources are matching within a reasonable tolerance since the correlation coefficient between the PIV wake positions and synchronous low-pass-filtered hot wire wake positions is about 0.85 on 450 samples. The wake centre series from hot wire data clearly exhibits a low-frequency variation with an added higher frequency “noise” that can be low-pass-filtered.

A 55P61 DANTEC hot wire X-probe is located 1D upstream of the wind turbine model of interest, measuring the horizontal components of the velocity. The longitudinal velocity u measured by the hot wire probe is also impacted by the vertical velocity, which is a common technical limitation of two-component hot wire measurements. On the other hand, the transverse velocity v is obtained by the difference of the effective velocities measured by each wire, and the influence of the vertical velocity w is consequently

**Fig. 5** Comparison of the wake centre position time series obtained from the PIV system and from the hot wire rake

negligible. Additionally, since the vertical velocity fluctuations have less amplitude than the horizontal ones, this is not expected to affect significantly the results shown. The wind turbine model of interest is fixed on a 6-axis aerodynamic balance (ATI Mini40), which is located underneath the floor. The three components of the aerodynamic force (F_x , F_y , F_z) and the three components of the associated torque (T_x , T_y , T_z) computed according to the centre of the rotor model are measured. The six channels of the aerodynamic balance are also acquired with the hot wire time series so as to allow time correlations.

A second wind turbine model can be installed 5D upstream of the model of interest for the configuration of disturbed upstream flow (case 7). The tested configurations are represented on Fig. 6, and the various parameters are summarized in Table 2. A photograph of the set-up is shown on Fig. 7.

3 Results and discussion

3.1 Spectral content

Figure 8 (left) presents the frequency-weighted power spectral density (PSD) of the transverse velocity fluctuations measured at undisturbed locations, upstream and downstream of the wind turbine model of interest. Here, the frequency is non-dimensionalized as a Strouhal number based on the wind turbine model diameter and the free-stream mean velocity at hub height. The PSDs are representative of turbulent flows; the energy is distributed over a broad frequency range without any distinctive peak, and the turbulent inertial sub-range is characterized by a linear slope of $-2/3$ on a log-scale plot; in other words the PSD is asymptotically proportional to $f^{-2/3}$ in this range.

Fig. 6 Experimental set-up. The wind turbine model of interest is the downstream one. The upstream turbine is only added for case 7 in order to generate a disturbed incoming flow on the downstream turbine

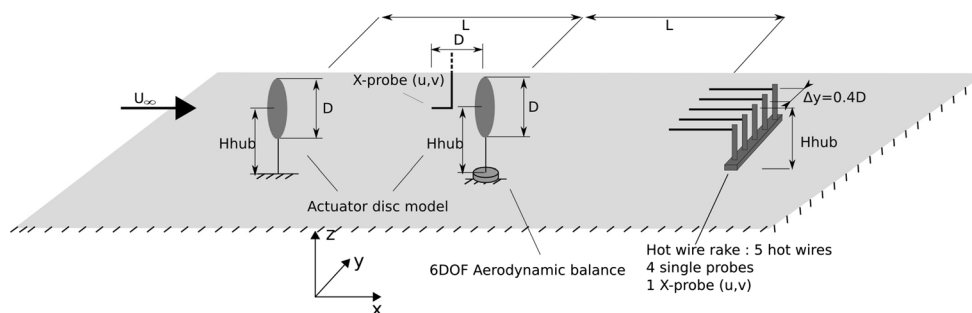


Table 2 Tested configurations

Case	D (m)	H_{hub}/D	L/D	a/D	Incoming flow	Balance measurements
Case 0 (validation)	0.1	0.1	4	0.33	Undisturbed	No
Case 1	0.1	1.25	3	0.4	Undisturbed	No
Case 2	0.1	1.25	4	0.4	Undisturbed	No
Case 3	0.1	1.25	5	0.4	Undisturbed	No
Case 4	0.2	0.625	4	0.4	Undisturbed	No
Case 5	0.2	0.625	5	0.4	Undisturbed	No
Case 6	0.2	1	5	0.5	Undisturbed	Yes
Case 7	0.2	1	5	0.5	Disturbed by an incoming wake	Yes



Fig. 7 Photograph of the experimental set-up (case 7). The traverse system holds the upstream hot wire, and may be moved in front of the hub of the downstream turbine during the acquisition

On the other hand, the PSD of the horizontal wake position fluctuations captured at $x/D = 5$ (Fig. 8, right; undisturbed inflow) differs from the classical turbulence PSD very distinctively in the low-frequency region, up to approximately $fD/U_\infty \approx 0.5$ where the slope of the PSD matches

that of the turbulent inertial sub-range. This region of increased power is assumed to be representative of the meandering of the wake. The cut-off value $fD/U_\infty = 0.5$ relates to an eddy scale of about two disc diameters, as suggested by Larsen et al. (2008). Above $fD/U_\infty = 0.5$, the PSD is analogous to that of the flow turbulence. This is a consequence of our process being also subject to the small scales of the flow turbulence. Indeed variations caused by a small eddy passing over only one wire will be picked up and will slightly modify the resulting wake position. Those variations are however dampened in the averaging process described by Eq. (1), and their amplitude does not compare with the larger-scale variations associated with the meandering.

It is noticeable that this meandering signature is amplified when the incoming flow is disturbed by the presence of a wind turbine model $5D$ upstream. Indeed, the power spectral density of the horizontal wake position fluctuations for the disturbed incoming flow presents even more energy in the low-frequency range than for the undisturbed incoming flow, though the cut-off frequency is similar. One could have expected an opposite behaviour, representative of the destruction of the turbulent structures, but the present results shows that the meandering process is maintained and even strengthened for cumulative wind turbine wakes.

3.2 Coherence between velocity fluctuations and instantaneous wake positions

In order to assess the relationship between upstream large-scale turbulence and wake meandering, the coherence

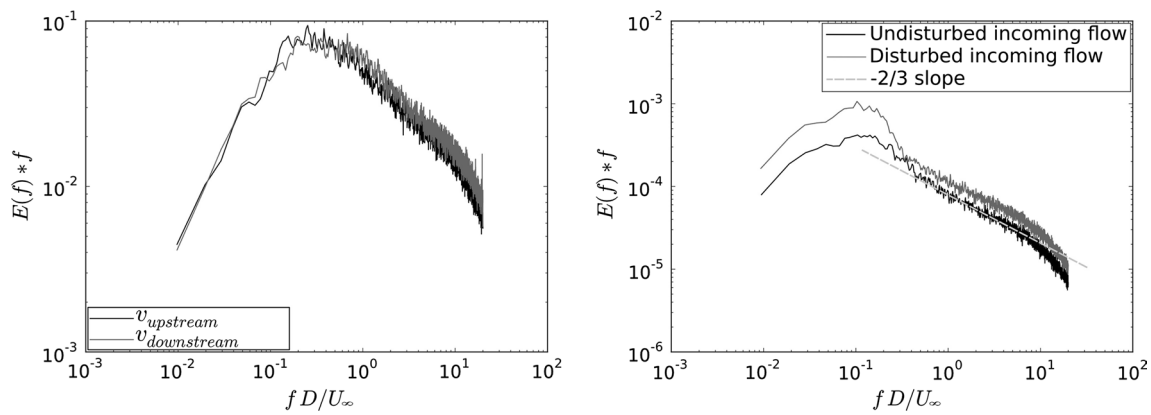


Fig. 8 On the left power spectral densities of the transverse velocity fluctuations at $(X/D = -1, y/D = 0)$ upstream of the disc of interest and at $(x/D = 5, y/D = 1)$ downstream of the disc for case 6. On the right PSDs of the horizontal wake position fluctuations at $x/D = 5$

for an undisturbed (no wake) incoming atmospheric flow (case 6) and for a disturbed incoming flow (one wind turbine model is located upstream of the model of interest, case 7)

between the upstream transverse velocity $v_{upstream}$ and the wake position y_{wake} is computed and shown on Fig. 9 (case 2). The coherence is defined as a dimensionless value deduced from the cross-spectrum and in the range between 0 (no correlation) and 1 (full correlation), as a function of the frequency.

The coherence is very high for the low frequencies up to about $fD/U_\infty = 0.1$. Between $fD/U_\infty = 0.1$ and $fD/U_\infty = 0.35$, the coherence decreases progressively until it reaches 0. The phase of the $v_{upstream}$ and y_{wake} coherence is perfectly linear up to $fD/U_\infty = 0.35$. Above this value, the phase is increasingly irregular, which is related to the absence of significant coherence. The linear evolution of the phase with the frequency is representative of a convective process, in agreement with the present assumptions that the meandering process is due to travelling turbulent eddies coming from the incoming flow and impacting the wind turbine wake as a whole.

The phase of the $v_{downstream}$ and y_{wake} coherence is constant, except for the very low-frequency range, indicating that their correlation is representative of a stationary phenomenon, in opposition to the convective process that affects the correlation between $v_{upstream}$ and y_{wake} .

It is also obvious from the present coherence distribution that the loss of correlation between the incoming turbulent flow and the meandering process is progressive and continuous. The validity limit of the frozen turbulence assumption, the nonlinear aspects of the relation between upstream velocity and wake position are responsible for this. It must be mentioned that the measurement error and the method used to calculate the position of the wake might also affect the results. In fact the position of the wake is not a precisely defined notion, and other authors might choose to calculate it in a different way.

Larsen et al. (2008) make the assumption that the wake of a wind turbine is a passive tracer of the incoming

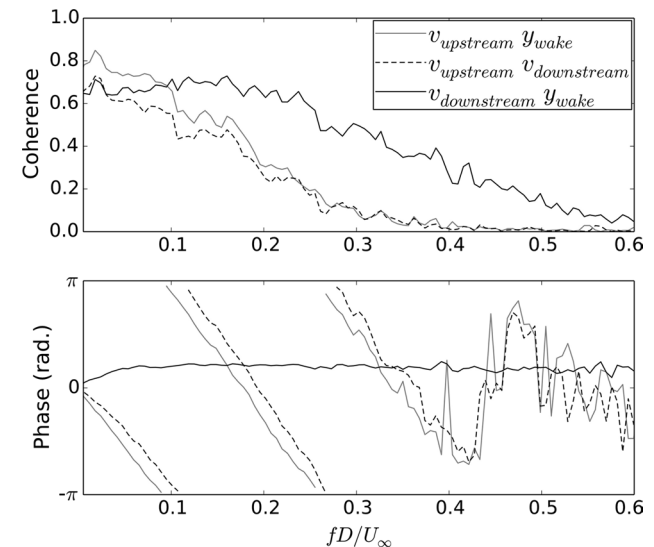


Fig. 9 Coherence and phase between $v_{upstream}$, $v_{downstream}$ and y_{wake} (case 2). The discontinuities of the phases are a graphing artefact due to the representation of an angular value on a Cartesian plot

turbulent eddies larger than twice the wake diameter, which would imply that the coherence would be equal to one up to $fD/U_\infty = 0.5$, and zero for higher Strouhal numbers. The coherence distribution shown here diverges from this assumption in several ways. Firstly the maximum coherence level is lower than one, which implies that the relationship between the upstream transverse velocities, and the wake position is not entirely linear, which is what is effectively measured by the spectral coherence. Secondly the coherence decreases progressively with the frequency and not as a discrete step. Thirdly, it is found that the coherence becomes negligible for a frequency value of $fD/U_\infty = 0.35$ instead of $fD/U_\infty = 0.5$.

The limit of $fD/U_\infty = 0.35$ between the partially correlated range and the uncorrelated range on Fig. 9 is noticeably lower than the previously discussed maximum frequency of the meandering deduced from the wake PSD on Fig. 8, which was found to be approximately $fD/U_\infty \approx 0.5$. This suggests that there are some frequencies found in the meandering that are not correlated with upstream flow turbulence.

The coherence and the associated phase between v_{upstream} and $v_{\text{downstream}}$ (Fig. 9) very closely mirror the coherence between v_{upstream} and y_{wake} . This can be interpreted as the sign that turbulent eddies large enough to subsist across the wind turbine model are all affecting the meandering of the wake.

The coherence between $v_{\text{downstream}}$ and y_{wake} further supports this assumption by showing features similar to those of the coherence between v_{upstream} and y_{wake} , except for the fact that the transitional range is slightly offset in the direction of increasing fD/U_∞ . The limit between the partially correlated and uncorrelated range limit now takes place at $fD/U_\infty = 0.5$, similar to the limit observed on the PSD of the horizontal wake position (Fig. 8, right). This suggests that contrarily to the v_{upstream} and y_{wake} cross-spectrum, the $v_{\text{downstream}}$ and y_{wake} cross-spectrum is representative of all the scales involved in the meandering.

It is found that the meandering frequency range extends up to $fD/U_\infty = 0.5$, while the highest bound of the coherent range between the wake meandering and the upstream velocity only extends up to $fD/U_\infty = 0.35$. In the hypothesis where the meandering is directly related to the transverse velocity fluctuations, it is expected that the coherence between the upstream transverse velocity and the wake position matches that of the upstream transverse velocity with the downstream velocity itself. The lack of coherence between the position of the wake and the upstream velocity for frequencies comprised in the range between 0.35 and 0.5, corresponding to scales of two to three times the diameter of the wind turbine model, is likely to be an effect of the turbulence produced in the vicinity of the wind turbine model itself. In addition, smaller turbulent structures have a faster change rate due to turbulent production and dissipation and will show lower coherence after a given convection distance. A parametric study has been performed in order to determine the influence of the diameter of the disc and the streamwise measurement distance on the coherence between the wake position and the upstream velocity (Fig. 10) (cases 2–5). It is shown that the coherence level only slightly decreases while the streamwise distance between the incoming flow measurements and the wake tracking location increases, since the turbulent eddies are more distorted during their longer travel (validity limit of the Taylor frozen turbulence). In any case, the level of coherence remains significant. These results could be used

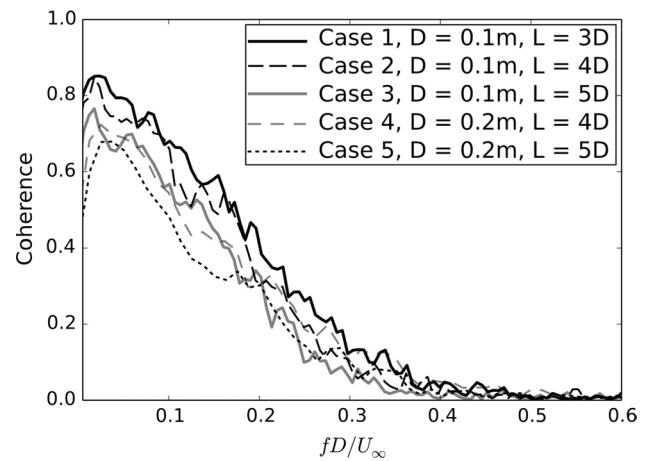


Fig. 10 Parametric study of the coherence between v_{upstream} and y_{wake} for different cases

to build some more realistic transfer functions between the incoming flow and the wake meandering than the ones currently used in Larsen et al. (2008, 2013), for instance.

3.3 Coherence between global load fluctuations and instantaneous wake positions

Having a real-time access to the incoming flow properties for full-scale wind turbines starts being conceivable thanks to the modern measurement equipment like nacelle-mounted LiDAR systems since they are able to capture the incoming instantaneous flow several hundred meters upstream of the rotor. On the other hand, one can expect that other physical values, like global wind turbine loads, could be also good candidates to predict the wind turbine wake meandering. Indeed, the incoming turbulent eddies impact the wind turbine and generate some load fluctuations that must be therefore correlated with the incoming velocity fluctuations and consequently, with the downstream wake position fluctuations. Additionally, these loads could be considered as spatially integrated information, since they are the result of the integration of the inhomogeneous aerodynamic loads all over the rotor, in contrast with the upstream velocity measurement which is local. This process can be assimilated to a low-pass filter that dampens the signature of high-frequency velocity fluctuations that cannot contribute to the meandering. Since only the horizontal meandering is studied, only the related lateral force F_y and yawing torque T_z loads are considered. For this part, a disc diameter of $D = 200$ mm is used.

Figure 11 (left) shows the coherence between the lateral force and the horizontal wake position for an undisturbed incoming flow (case 6). A significant coherence level is obtained for frequencies lower than $fD/U_\infty \approx 0.35$. It shows how the large turbulent eddies contained in the

approach atmospheric flow modify the instantaneous wind direction and generate consequently some fluctuations of the global lateral force on the actuator disc. The current cut-off frequency is equivalent to the one obtained for the coherence with the upstream velocity. Consequently, the lateral force on the wind turbine could also be a good candidate to predict in real time the downstream wake meandering. This value may be more easily accessible than the upstream velocity in a wind plant.

Figure 11 (right) shows the coherence between the lateral force and the horizontal wake position for a disturbed incoming flow (a wind turbine model is located $5D$ upstream of the wind turbine model of interest). The coherence is similar for both configurations (undisturbed and disturbed approach atmospheric flows) even if the “cut-off” frequency is slightly smaller in the disturbed inflow case. This difference is likely due to the lower local average velocity in the two turbine case, considering the frequency is non-dimensionalized by the average velocity at

the infinite upstream in both cases (the velocity at the hub for both turbines is not directly available).

Figure 12 (left) shows that the coherence between the yawing torque and the horizontal wake position is not significant for an undisturbed incoming flow (case 6). On the other hand, the coherence between the yawing torque and the horizontal wake position is significant in the disturbed inflow configuration (Fig. 12, right). This is an unexpected result. In order to explain it, two assumptions are made:

Firstly, it is assumed that the yawing loads on a turbine are correlated with perturbations from a meandering wake of another turbine in the inflow. The mechanism could be described as follow: as the wake of the upstream wind turbine model meanders, it impacts the model of interest with an unsteady behaviour, sometimes on the left, sometimes on the right, and sometimes centred. That unbalances the aerodynamic loads between the left and the right part of the rotor, generating a yawing torque.

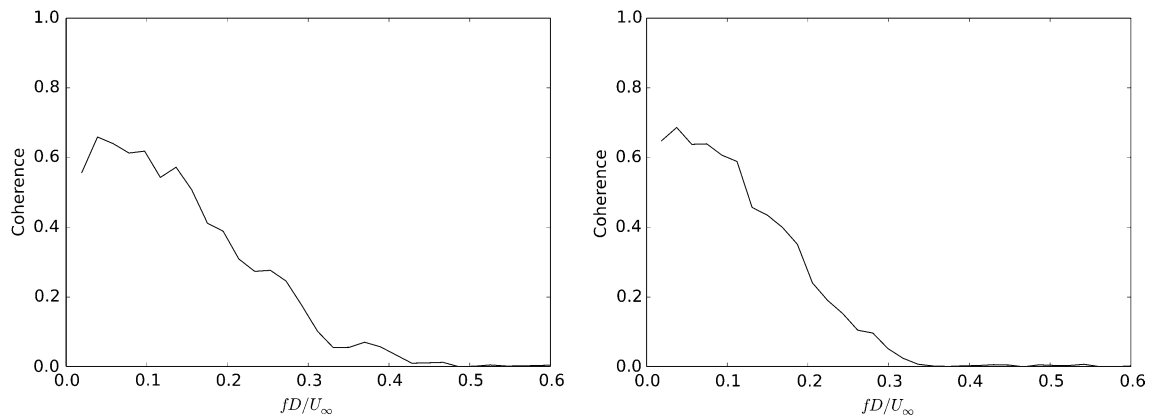


Fig. 11 Coherence between the wake position and the lateral force F_y , for the undisturbed approach atmospheric flow (case 6, left) and for the disturbed approach flow (case 7, right)

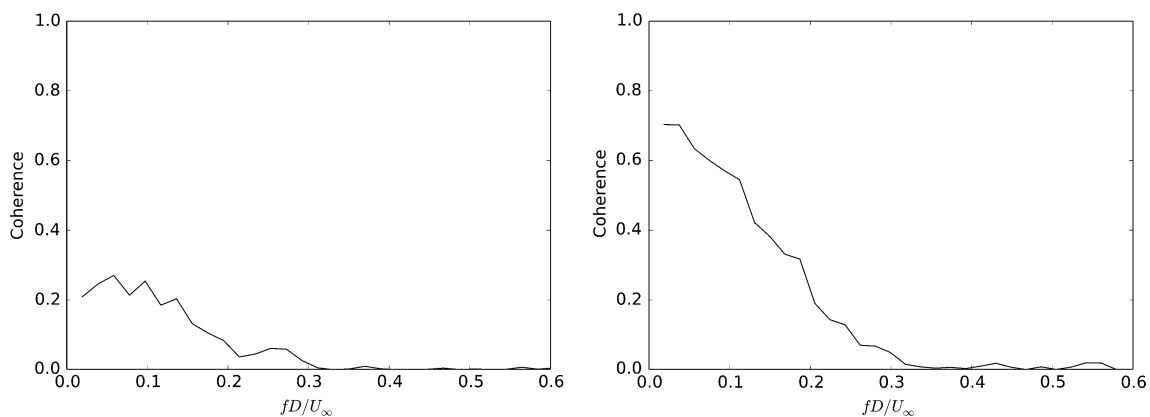


Fig. 12 Coherence between the wake position and the yawing torque T_z for the undisturbed approach atmospheric flow (case 6, left) and for the disturbed approach flow (case 7, right)

Secondly, it is assumed that when two turbines are aligned with the main flow direction, their respective wakes downstream of the second turbine are superimposed (at least partially). This follows from the assumption that both wakes are affected by the same large-scale fluctuations of the transverse velocity. This is in agreement with the PSDs on Fig. 8 (right) which show that the low-frequency fluctuations of the measured position of the wake are stronger in the double wake case.

If both assumptions are valid, then there is correlation between the position of the two superimposed wakes and the yawing torque on the downstream turbine, even though there is no significant correlation between the yawing torque and the position of the wake in a single turbine case, which is what Fig. 12 shows.

Ideally the coherence between the position of the wake of the first turbine and the yawing torque on the second turbine or between the positions of both wakes would be measured directly, but this is not feasible with the current set-up since the hot wire rake is too intrusive to be positioned between the two discs.

4 Conclusion

The present work proposed an experimental methodology to characterize the unsteady properties of a wind turbine model wake and particularly its ability to follow the large-scale motions induced by large turbulent eddies contained in the approach flow. The measurements were performed in the wind tunnel of the PRISME Laboratory of the University of Orléans, where a neutrally stratified atmospheric boundary layer on a moderately rough terrain was modelled at a reduced scale of 1:400. Preliminary measurements ensured that the flow had the right properties, according to the atmospheric literature and that the incoming turbulence length scales were larger than the wind turbine model (based on actuator disc concept). The results are expected to scale up to full-scale configurations where wind turbine wakes located in atmospheric boundary layer were observed to experience a similar meandering. This phenomenon was illustrated in the present work by the build-up of energy in the PSD of the horizontal meandering up to a non-dimensionalized frequency of $fD/U_\infty = 0.5$ (turbulent length scales twice larger than the wind turbine model diameter).

It has been shown that the instantaneous horizontal wake position correlates well with the upstream transverse velocity for wavelength larger than three times the disc diameter, whereas it does not correlate at all for wavelength smaller than twice the disc diameter. The presence of the wind turbine model itself tends to distort the intermediate turbulent length scales, destroying the coherence between these

particular length scales, as seen on the coherence of the velocity measured upstream and downstream of the wind turbine model. It is then concluded that the wake is actually a rather passive tracer of the large surrounding turbulent structures, although the measured coherence levels suggest that the relationship between the inflow and the wake position is not entirely linear either.

The parametric study for different disc diameters and downstream distances has shown that the coherent frequency range between the transverse velocity and the horizontal wake meandering seems to be rather invariant and extends approximately up to $fD/U_\infty = 0.35$. A slight decrease of coherence is observed with the increasing distance of meandering tracking due to the loss of coherence and the distortion of the turbulent eddies themselves during the increased advection distance.

The fluctuations of the lateral force and of the yawing torque affecting the wind turbine model were measured and correlated with the wake meandering. Two approach flow configurations were then tested: an undisturbed incoming flow (modelled atmospheric boundary layer) and a disturbed incoming flow, with a wind turbine model located 5D upstream of the wind turbine model of interest.

Results showed that the meandering process is amplified by the presence of the upstream wake, since the signature of the meandering of the transverse wake position is strengthened on the PSD of the position of the wake.

It has been shown that the coherence between the lateral force and the horizontal wake position is significant up to $fD/U_\infty = 0.5$. This leads to the conclusion that the lateral force is a better candidate than the transverse velocity to predict in real time the meandering process, since the coherent frequency range between the position of the wake and the lateral force is wider than for the coherence with the upstream velocity. It is likely that the correlation with the meandering process is better because the loads are space-averaged indicators of the velocity fluctuations that impact the rotor.

On the other hand, the fluctuations of the yawing torque cannot be used as a predictor of the meandering since they do not correlate directly with the downstream meandering process, but it is a good indicator of the presence of a meandering wake in the inflow. These results indicate that monitoring global lateral force and yawing torque on wind turbines, which seems easier than monitoring the upstream velocity, could help to predict the meandering process and its consequences on following wind turbines. The results shown may be used to build numerical models of the meandering process and to implement them in wind turbine control strategies to improve the wind farm monitoring and performance in real time, potentially allowing for active load alleviation by pitch or yaw actuation.

References

- Ainslie JP (1988) Calculating the flow field in the wake of wind turbines. *J Wind Eng Ind Aerodyn* 27:213–224
- Aubrun S, Devinant P, España G (2007) Physical modelling of the far wake from wind turbines. Application to wind turbine interactions. In: Proceedings of the European wind energy conference, Milan, Italy
- Aubrun S, Loyer S, Hancock PE, Hayden P (2013) Wind turbine wake properties: comparison between a non-rotating simplified wind turbine model and a rotating model. *J Wind Eng Ind Aerodyn* 120:1–8
- Bingöl F, Mann J, Larsen GC (2010) Light detection and ranging measurements of wake dynamics. Part 1: one-dimensional scanning. *Wind Energy* 13:51–61
- Cannon S, Champagne F, Glezer A (1993) Observations of large-scale structures in wakes behind axisymmetric bodies. *Exp Fluids* 14(6):447–450
- Chamorro LP, Hill C, Morton S, Ellis C, Arndt REA, Sotiropoulos F (2013) On the interaction between open channel flow and an axial-flow turbine. *J Fluid Mech* 716:658–670
- Cholbrock AK, Fleming PA, Fingersh LJ, Wright AD, Schlipf D, Haizman F, Belen F (2013) Field testing LiDAR based feed-forward controls on the NREL controls advanced research turbine. Conference Paper NREL/CP-5000-57339
- Counihan J (1975) Adiabatic atmospheric boundary layers: a review and analysis of data from the period 1880–1972. *Atmos Environ* 9:871–905
- Davoust S, Jehu A, Bouillet M, Bardon M, Vercherin B, Scholbrock A, Fleming P, Wright A (2014) Assessment and optimization of LiDAR measurement availability for wind turbine control. In: Scientific. Proceedings of EWEA Conference March 10–13, 2014, Barcelona, Spain
- Engineering Sciences Data Unit (1985) Characteristics of atmospheric turbulence near the ground. Item No. 85020
- España G, Aubrun S, Loyer S, Devinant P (2011) Spatial study of the wake meandering using modelled wind turbines in a wind tunnel. *Wind Energy* 14:923–937
- España G, Aubrun S, Loyer S, Devinant P (2012) Wind tunnel study of the wake meandering downstream of a modelled wind turbine as an effect of large scale turbulent eddies. *J Wind Eng Ind Aerodyn* 101:24–33
- Felli M, Camussi R, Di Felice F (2011) Mechanisms of evolution of the propeller wake in the transition and far fields. *J Fluid Mech* 682:5–53
- Frandsen S, Barthelme R, Pryor S, Rathmann O, Larsen S, Højstrup J, Thøgersen M (2006) Analytical modelling of wind Speed deficit in large offshore wind farms. *Wind Energy* 9:39–53
- Hancock PE, Pascheke F (2014) Wind tunnel simulation of the wake of a large wind turbine in a stable boundary layer: part 2 the wake flow. *Bound Layer Meteorol* 151:23–37
- Hu H, Yang Z, Sarkar P (2012) Dynamic wind loads and wake characteristics of a wind turbine model in an atmospheric boundary layer wind. *Exp Fluids* 52:1277–1294
- Iungo GV, Viola F, Camarri S, Porté-Agel F, Gallaire F (2013) Linear stability analysis on wind turbine wakes performed on wind tunnel measurements. *J Fluid Mech* 737:499–526
- Jensen NO (1983) A note on wind generator interaction. Risø Report M-2411
- Kaimal JC, Finnigan JJ (1994) Atmospheric boundary layer flows, their structure and measurements. Oxford University Press, Oxford
- Larsen GC, Madsen HA, Thomsen K, Larsen TJ (2008) Wake meandering—a pragmatic approach. *Wind Energy* 11:377–395
- Larsen TJ, Madsen HA, Larsen GC, Hansen KS (2013) Validation of the dynamic wake meander model for loads and power production in the Egmond aan Zee wind farm. *Wind Energy* 16(4):605–624
- Medici D, Alfredsson PH (2006) Measurements on a wind turbine wake: 3D effects and bluff body vortex shedding. *Wind Energy* 9:219–236
- Snyder WH (1981) Guideline for fluid modelling of atmospheric diffusion. US Environmental Protection Agency. Report EPA-600/8-81-009
- Taylor GJ, Milborrow DJ, McIntosh DN, Swift-Hook DT (1985) Wake measurements on the Nibe windmills. In: Proceedings of the 7th British wind energy association conference March 27–29 1985, Oxford
- Trujillo JJ, Kühn M (2009) Adaptation of a lagrangian dispersion model for wind turbine wake meandering. In: Proceedings of the EWEA conference, March 16–19, Marseille, France
- Trujillo JJ, Bingöl F, Larsen GC, Mann J (2011) Light detection and ranging measurements on wake dynamics, part II: two-dimensional Scanning. *Wind Energy* 14:61–75
- VDI guideline 3783/12 (2000) Physical modelling of flow and dispersion processes in the atmospheric boundary layer—application for wind tunnels. Beuth Verlag, Berlin
- Zhang W, Markfort CD, Porté-Agel F (2012) Near-wake flow structure downwind of a wind turbine in a turbulent boundary layer. *Exp Fluids* 52:1219–1235
- Zhang W, Markfort CD, Porté-Agel F (2013) Wind turbine wakes in a convective boundary layer: wind tunnel study. *Bound Layer Meteorol* 146:161–179